Article

NiFe Layered Double Hydroxide Electrocatalyst Prepared via an Electrochemical Deposition Method for the Oxygen Evolution Reaction

Murugesan Praveen Kumar [1,*,†], Moorthy Sasikumar [2,†], Arunachalam Arulraj [1,3], Venugopalan Rajasudha [4], Govindhasamy Murugadoss [5,*], Manavalan Rajesh Kumar [6], Shaik Gouse Peera [7,*] and Ramalinga Viswanathan Mangalaraja [1,*]

1   Faculty of Engineering and Sciences, Adolfo Ibáñez University, Diagonal las Torres 2640, Peñalolén, Santiago 7941169, Chile
2   Department of Physics, Bishop Heber College, Thiruchirapalli 620023, Tamil Nadu, India
3   Departamento de Física, Facultad de Ciencias Naturales, Universidad de Atacama, Av. Copayapu 485, Copiapó 1531772, Chile
4   Department of Chemistry, Annai Vailankanni Arts and Science College, Thanjavur 613007, Tamil Nadu, India
5   Centre for Nanoscience and Nanotechnology, Sathyabama Institute of Science and Technology, Chennai 600119, Tamil Nadu, India
6   Institute of Natural Science and Mathematics, Ural Federal University, 620002 Yekaterinburg, Russia
7   Department of Environmental Science, Keimyung University, 1095 Dalgubeol-daero, Dalseo-gu, Daegu 42601, Republic of Korea
*   Correspondence: praveenkumarmurugesan280589@gmail.com (M.P.K.); murugadoss_g@yahoo.com (G.M.); gouse@kmu.ac.kr (S.G.P.); mangal@uai.cl (R.V.M.)
†   These authors contributed equally to this work.

Abstract: Herein, we aimed to obtain NiFe layered double hydroxide (LDH) with a controlled phase and surface morphology as a highly active and stable oxygen evolution catalyst via the electrochemical deposition method, which was thermodynamically stable for the oxygen evolution reaction (OER) in an alkaline medium. The NiFe-LDH sample was analyzed by sophisticated instruments and tested as an electrocatalyst on Toray carbon (TC). The NiFe-LDH electrocatalyst showed an excellent performance with lower overpotential of 0.27 V at 35 mA cm^{-2} and higher density of 125 mA cm^{-2} for OER in the 1 M KOH electrolyte solution. Moreover, the prepared catalyst exhibited unpredictable long-time stability for 700 h. From our knowledge, NiFe-LDH is a robust highly stable electrocatalyst compared to the recent reports.

Keywords: OER; NiFe-LDH electrocatalyst; electrochemical deposition; (Oxy)hydroxides phases; long-time stability

1. Introduction

Hydrogen energy is regarded as one of the major chemical forms of energy for various applications ranging from domestic to transportation sectors. [1,2]. A promising method of producing hydrogen is by electrochemical splitting of water into hydrogen and oxygen [3,4]. By electrochemical water splitting, high purity hydrogen can be produced. In addition, electrochemical water splitting is considered as an environmentally friendly technique with nearly no carbon emissions. Typically, the water splitting process combines the following two half-cell reactions happening on anodes and cathodes, respectively: (i) the oxygen evolution reaction (OER): $4OH^- \rightarrow O_2 + 2H_2O + 4e^-$ and (ii) the hydrogen evolution reaction (HER): $2H_2O + 2e^- \rightarrow H_2 + 2OH$ [5–7]. The OER, also referred to as water oxidation, is a complex process from the kinetic perspective since it limits the overall efficiency of water splitting and is a multi-proton-coupled four-electron-transfer reaction [8–11]. Consequently, discovering an effective electrocatalyst is key for enhancing the sluggish OER kinetics [12]. Exploring new electrocatalytic materials with durable electrodes is crucial for the effective

application of water splitting technology. In this regard, in recent years, the development of highly active and abundant earth-transition metals such as Co-, Ni-, Fe-, and Mn-based oxides, hydroxides, and phosphides has been explored [13]. In addition, bimetallic composite hydroxides outperform single-metal catalysts in electrocatalysis. It has been suggested that the presence of iron components can boost the OER activity of nickel- or cobalt-based oxide/hydroxide composites. Furthermore, iron is one of the most effective non-precious OER catalysts and exhibits very high activity [14]. However, relatively few studies have examined the impact of NiFe-based (oxy)hydroxides on the OER catalytic mechanism. Iron's effect on the catalytic activity of Ni catalysts remains largely undetermined. Recent studies have suggested that synergistic interactions between Fe and Ni (oxy)hydroxides and high oxidation states of the Fe and Ni centers are responsible for the good activity [15–18]. Additionally, it has been noted that there is a linear correlation between the iron surface coverage and the OER activity of Fe-based (oxy)hydroxide, highlighting the importance of surface Fe species in OER electrocatalysis [19]. Additionally, the iron impurities in the electrolytes, which take the form of free ions, may also influence the electrocatalytic activity during the water splitting reaction (within the concentration range of ppb to ppm). However, such Fe adsorption effect on OER activity is unknown. Notably, theoretical simulations have demonstrated that phosphate groups [20], N sites [21], and electronegative substrates [22] could increase the OER activity by promoting the partial electron removal from the active centers. Fe ions are expected to contribute a significant amount of electronegative surface at this situation and may tend to promote the electrocatalytic activity (NiFe-based catalysts) by a similar electron-transfer mechanism. Xiang et al. [23] explained that NiFe-LDH with a hydroxide interfacial layer displays enhanced activity for OER. The synergistic effect between NiFe-LDH and the hydroxide layer stimulates a sympathetic local chemical environment with the appropriate electronic structure, which directs optimal OH intermediates' adsorption, and that could enhance the OER activity. This is one of the primary motivations for this current work.

As previously stated, the development of novel electrocatalytic materials and their preparation method, as well as the type of electrodes used, are crucial factors influencing the electrochemical reactions during the application of water splitting. Currently, sol-gel synthesis, colloidal synthesis, zeolitic imidazolate frameworks, and solvo- (or) hydrothermal procedures are among the solution-based techniques, which are the most frequently used method to synthesize the NiFe (oxy)hydroxides electrocatalyst [24–33]. However, there are some significant problems with the catalyst efficacy with solution-based techniques such as (i) limited control over nanomaterial size; (ii) uneven catalyst loading and distribution over conductive substrates (such as carbon cloth, nickel foam, or Toray carbon); and (iii) lack of methods to track crystal growth in real time during synthesis. In this context, the electrochemical deposition technique has emerged as a promising method for synthesizing electrocatalysts with precise control over the nanomaterials' size and with even catalyst distribution on the conductive surfaces. Moreover, electrochemical deposition does not require any complicated experimental requirements such as high pressure/temperature. In addition, electrochemical deposition makes it possible to control the growth process of nanomaterials while simultaneously increasing their degree of irreversibility by interatomic interactions. Additionally, electrochemical deposition is a simple process that has the potential for scale up into large-scale industrial production [34].

Herein, the electrochemical deposition of NiFe-LDH has been carried out over the Toray carbon (TC) (as cathode) and graphite sheet (as anode) in the electrochemical setup. The fabricated NiFe-LDH on Toray carbon has been used as an active electrocatalyst for the efficient splitting of water molecules (OER) in 1 M KOH. The electrochemically fabricated NiFe-LDH electrocatalyst showed an overpotential of 0.18 V for OER with excellent stability for over 700 h in the two-electrode system.

2. Results and Discussion

The XRD pattern of the Fe, Ni, and NiFe-LDH film deposited on the TC sheet is shown in Figure 1. The XRD peaks of Fe on the TC sample observed at 26.9, 44.8, 52.2, 54.9, and 76.8° corresponded to the (120), (400), (422), (221), and (533) planes, respectively. In addition, the XRD peaks represented the formation of $Fe(OH)_2$ (JCPDS no. 29-0713) and $\gamma\text{-}Fe_2O_3$ (JCPDS no. 39-1346) with cubic structure (Figure 1a) [35,36]. Meanwhile, the diffraction peaks appeared for the Ni sample at 26.7° (101), 38.4° (102), 44.6° (111), and 52° (200), which revealed the presence of Ni in the form of $Ni(OH)_2$ (JCPDS 14-0117) and the Ni matrix, as shown in Figure 1b [37]. Figure 1c shows the diffraction peaks corresponding to NiFe-LDH (JCPDS no 40-0215) at the two theta angles of 26.7°, 44.5°, and 54.5° corresponding to the (006), (018), and (110) planes for NiFe-LDH and 51.8° (200) and 76.2°(220) for Ni_3Fe, respectively [38]. Further, it was observed that the diffraction peaks of NiFe-LDH are shifted towards lower angles when compared to $Fe(OH)_2$ and $Ni(OH)_2$. The obtained XRD result clearly confirmed the formation of NiFe-LDH.
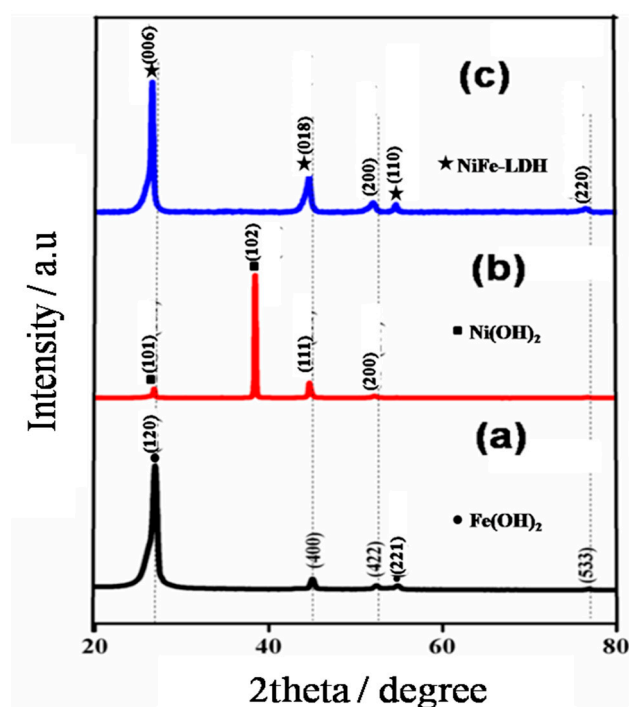

Figure 1. XRD pattern of (**a**) Fe, (**b**) Ni, and (**c**) NiFe-LDH film deposited on the TC sheet.

Figure 2 represents the Raman spectra of Fe, Ni, and NiFe-LDH on TC. The peaks appearing at 248, 300, 380, 490, 530, and 1311 cm^{-1} correspond to oxide species (Figure 2a). The peak of 658 cm^{-1} corresponds to the presence of vibrational bonds of Fe-O inγ-Fe_2O_3 [28,34]. The Raman peaks of 464, 795 and 985 cm^{-1} exhibit the formation of α-$Ni(OH)_2$ and the vibration of Ni-O for Ni on TC, respectively (Figure 2b). Furthermore, the Raman peaks of NiFe-LDH appeared at 472, 543, 689, and 1335 cm^{-1}. The peaks at 472 and 543 cm^{-1} are attributed to the formation of γ-NiOOH in NiFe-LDH; consequently, it clearly showed that the intensity of 543 cm^{-1} is higher than 472 cm^{-1}. Moreover, the Raman scattering peaks are observed at 689 and 1335 cm^{-1} for the vibrational bond of Fe_2O_3 for NiFe-LDH on TC. The Raman study further supported the structural modification in the NiFe-LDH, and it can promote the OER activity of Ni and Fe in an alkaline medium.
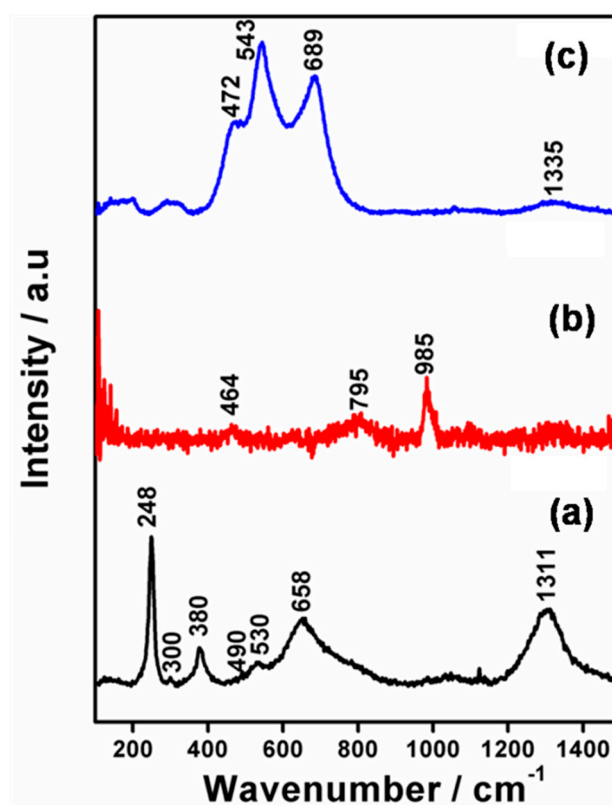
Figure 2. Raman spectra of (**a**) Fe on TC, (**b**) Ni on TC, and (**c**) NiFe-LDH deposited on TC sheet.

FE-SEM images demonstrated the surface morphology of Ni, Fe, and NiFe-LDH on TC, as shown in Figure 3. Figure 3a illustrates that the TC sheet was fully covered with Ni/Ni(OH)$_2$ nanosheets, which is in the range of ~100–200 nm. The self-protected Ni/Ni(OH)$_2$ nanosheets are uniformly formed during the electrochemical deposition process. Moreover, the FE-SEM image indicated that a nano-spike surface morphology for Fe was on the TC sheet, as shown in Figure 3b. Furthermore, Figure 3c shows TC has been uniformly covered with the Ni and Fe complex, which provided high surface area as well as active centers to support the water oxidation process. The formation of NiFe -LDH is shown clearly in Figure 3c.
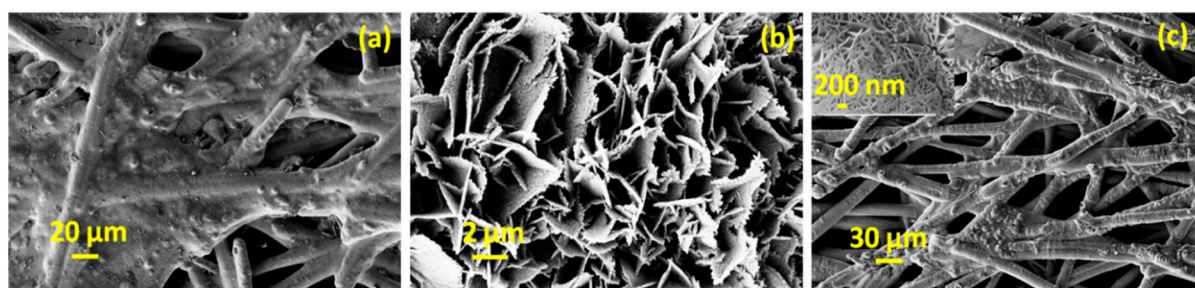

Figure 3. The FE-SEM images of (**a**) Ni-coated TC, (**b**) Fe-coated TC, and (**c**) NiFe-LDH formation on TC (insert shows high magnification image).

The HR-TEM images revealed the size and morphology of Ni, Fe, and NiFe-LDH on TC, as shown in Figure 4. In Figure 4a, Ni forms a nanosheet-like morphology with a size of 200 nm, which confirmed the sheet was protected on TC in the controllable size. Hence, the Fe nano-spikes were vertically grown onto the TC surface (Figure 4b). Furthermore, Figure 4b shows nano-spikes with sizes in the range of ~50–100 nm. The nano-spike can provide support to enlarge the surface area of Ni. Figure 4c shows theHR-TEM image

of NiFe-LDH on the TC surface, and the nano-spike of 100 nm in size with well-defined surface morphology is observed in Figure 4c. The SAED patterns of Ni, Fe, and NiFe-LDH are shown in Figure 4d–f, which confirm the materials have goodcrystallinity. Additionally, the HR-TEM images in Figure 4g–i show individual lattice fringes of 0.177 (Ni-200) and 0.312 ($Ni(OH)_2$ -101) for Ni, 0.180 (Fe-422) and 0.206 (Fe-400) for Fe, and 0.156 (NiFe-LDH) and 0.177 (NiFe-200) for NiFe-LDH, respectively. The HR-TEM result has proved the formation of (oxy)hydroxides in NiFe layered nanomaterial. The presence of elements was carried out by mapping and the creation of an EDAX spectrum of NiFe-LDH, as shown in Figure 5a–d.The images in Figure 5a–c exhibit the presence of Ni, Fe, and O, respectively. Figure 5d exhibits the presence of Ni, Fe, and O peaks in the NiFe-LDH and, further, it confirms the formation of binary metal oxides alloy compounds.
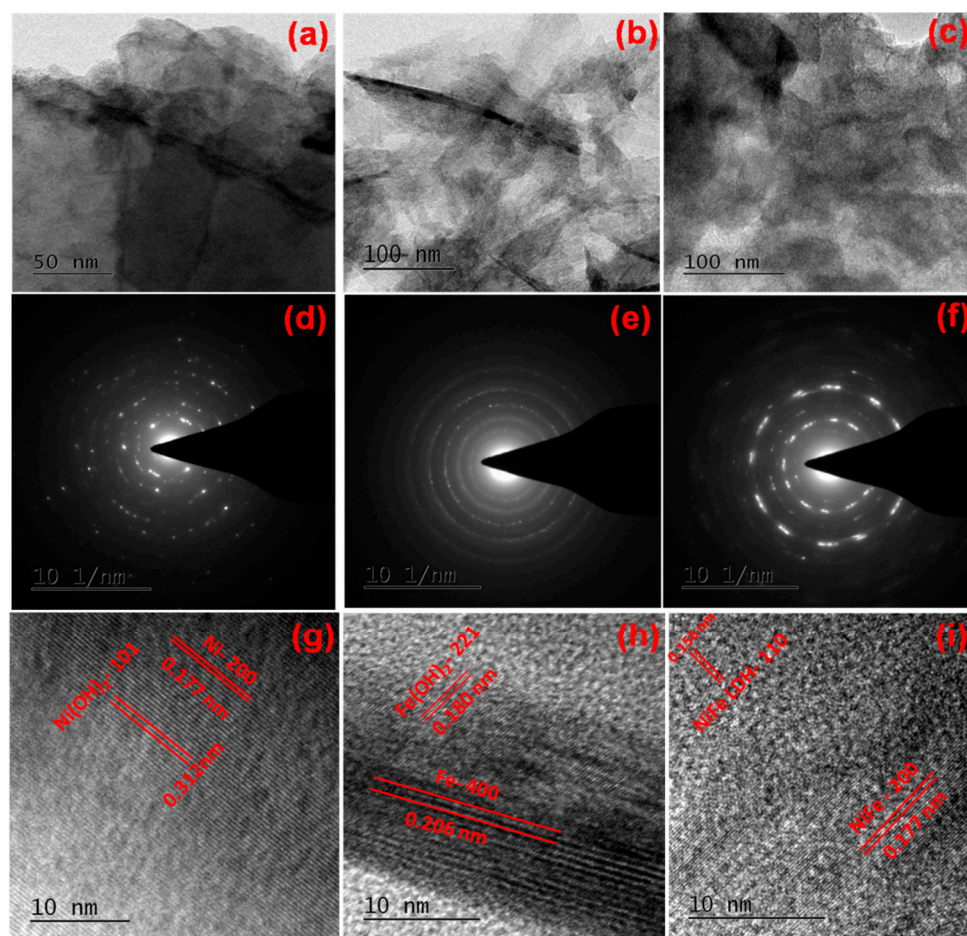
Figure 4. HR-TEM images (**a**–**c**), SAED pattern (**d**–**f**), and the corresponding lattice fringes (**g**–**i**) of Ni on TC, Fe on TC, and NiFe-LDH on TC, respectively.

The XPS study was examined to prove the presence of elements and the oxidation state of as-prepared Fe on TC, Ni on TC, and NiFe-LDH on TC, as shown in Figure 6. The high-resolution XPS spectrum of Ni on TC revealed that Ni's main peaks occurred at the binding energies of 859.8 and877.3 eV for $2p_{3/2}$ and for $2p_{1/2}$, respectively, as shown in Figure 6a. In addition, the satellite peaks were presented at about the binding energies of 865 and 883 eV for $2p_{3/2}$ and $2p_{1/2}$, respectively (Figure 6a). From the result, we clearly observed the presence of NiO on the TC sheet (Figure 6a). Figure 6b shows the high-resolution spectrum of Fe on TC; the peaks of Fe $2p_{3/2}$ and Fe $2p_{1/2}$ appeared at the binding energies of 711 and 723 eV, respectively, which confirmed that the iron exists in +3 oxidation states in the substrate of TC [39]. Furthermore, Figure 6c shows the survey spectrum of NiFe-LDH. The major peaks appeared at 859.1, 713.4, and 531.3 eV corresponding to Ni, Fe, and O elements,

respectively. The survey spectrum confirmed the presence of constituted elements in NiFe-LDH. Additionally, the high-resolution spectra of the Ni 2p and Fe 2p main peaks are displayed at the binding energies of 860 and 877.6 eV and 713.4 and 725.5 eV, respectively, which represent the presence of Ni and Fe in NiFe-LDH (Figure 6d,e). From the spectra, we identified that the peaks are slightly shifted towards higher binding energies compared to bare Ni and Fe, due to the formation of NiFe-LDH. Furthermore, Figure 6f shows the O1s high-resolution spectra, which shows that two major peaks appearing at 530.3 and 532.2 eV are attributed to metal hydroxides (M-OH) and intercalated water molecules into NiFe-LDH (H_2O), respectively [40].
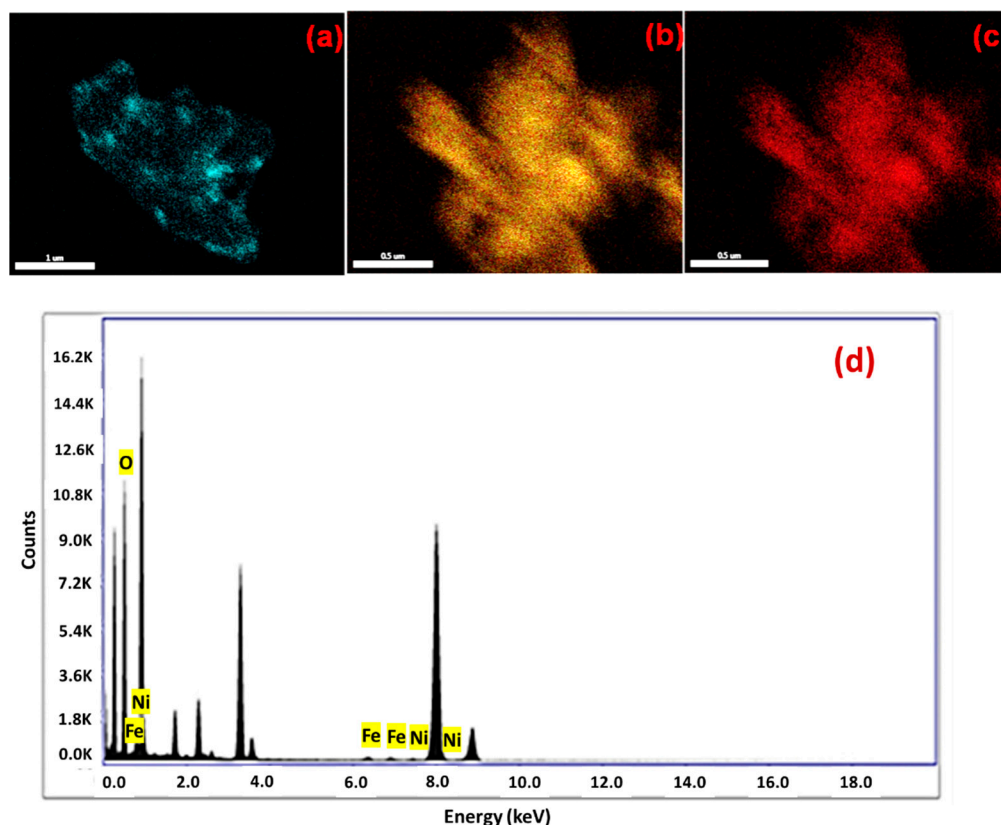
Figure 5. (**a**) Ni, (**b**) Fe, and (**c**) O HR-TEM elemental mapping and (**d**) EDAX spectrum of NiFe-LDH on TC.

The electrochemical studies were carried out by a conventional three-electrode system (NiFe-LDH as a working electrode, Pt wire as a counter electrode, and $Hg/HgSO_4$ as a reference electrode) in 1 M KOH electrolyte with a scan rate of 10 mV s^{-1} for the OER. For all the electrochemical measurements, the potential of Hg/HgO was changed into reversible hydrogen electrode (RHE) via the basic formula of [41],

$$E_{(RHE)} = E^0_{(Hg/HgO)} + E_{(Observed)} + 0.059(pH) \text{ V}$$

$$\text{Overpotential } (\eta) = E_{(RHE)} - 1.23 \text{ V}$$

We have quantified the catalysts' deposition on Toray carbon. The amount of the coating is 1 mg for all the three types of samples. Figure 7 shows the LSV curve of TC, Fe, Ni, and NiFe-LDH on TC. The NiFe-LDH exhibited the lowest onset potential of 1.41 V, which is lower than that of the bare TC (1.57 V), Fe on TC (1.53 V), and Ni on TC (1.52 V). The shifting of the redox peak at 1.45 V is due to change of electronic structure configuration, conductivity, and active sites in NiFe-LDH. Moreover, Gao et al. [42] observed that the Fe^{2+}-NiFe-LDH exhibits enhanced activity for the OER. Their theoretical survey proposed

that the Fe–O–Fe oxygen-bridged metal motifs have a beneficial effect on the catalysis for OER (where the Fe atom is judged as the active site), while the Fe–O–Fe couples can be built by the introduction of Ni-sited Fe atoms into NiFe-LDH, which could be active as stable high-valent motifs and that can enhance the OER intrinsic activity. At the onset potential of 1.5 V, NiFe-LDH displays a current density up to 35 mA cm^{-2}, which is one-fold higher in value than Fe on TC and Ni on TC. This result demonstrated the excellent improvement of the electrocatalytic activity toward OER. The combination of NiFe-LDH represented much lower onset potential than the Ni and Fe deposited on TC. This significant improvement of OER activity is due to the formation of (oxy)hydroxide phases in the NiFe-LDH electrocatalyst. Furthermore, Table S1 shows the comparison of the obtained result with reported results. In addition, we observed the Tafel values for all the as-prepared electrocatalysts as shown in Figure 7b. The Tafel slope value of NiFe-LDH is 0.095 V dec^{-1} in low overpotential ranges, which ismuch lower than that of Ni (0.237 V dec^{-1}) and Fe on TC (0.248 V dec^{-1}), demonstrating a faster kinetics reaction during the OER. Moreover, we have plotted the comparison of the onset potential, in which the onset potential at 35 mA cm^{-2} and overpotential for all electrocatalysts is shown in Figure 7c. From the comparison plot, the NiFe-LDH showed the lowest potential values compared to the others. We confirmed that the (oxy)hydroxide phases are very suitable for OER in an alkaline medium. The stability testing is another important key factor for estimating the electrocatalytic performance in an alkaline solution. Hence, the various chronopotentiometry measurements of 60, 50, 40, and 30 mA cm^{-2} were worked out to estimate the durability of NiFe-LDH. It showed no evident change in the onset potential for each 100 h test (Figure 7d) and validated the outstanding durability of the NiFe-LDH electrocatalyst for the OER in an alkaline electrolyte. It is important to note that after 700 h of chronopotentiometry measurement testing during OER in alkaline medium, only a 3% reduction from the starting potential was observed. This indicates that (oxy)hydroxide phases of the NiFe-LDH electrocatalyst are very suitable for water electrolysis technology, which will support the replacement of noble metals and reduce the cost of the water electrolyzer.
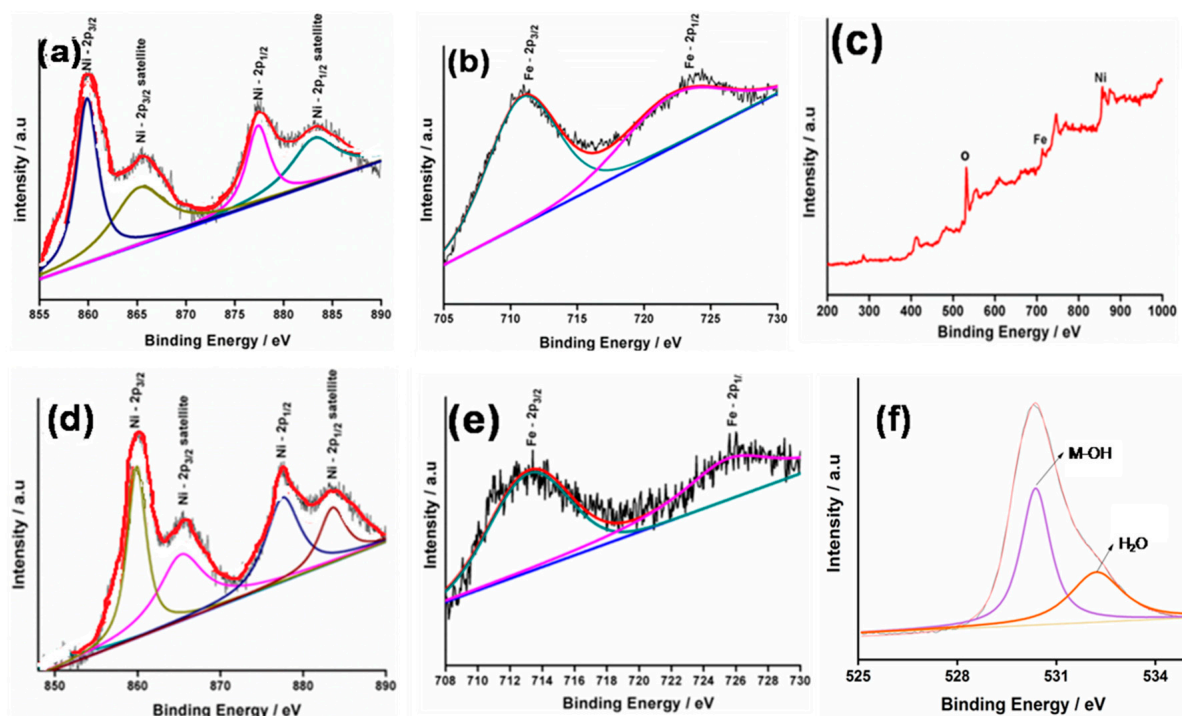

Figure 6. (**a**) Ni 2p and (**b**) Fe 2p XPS spectra, (**c**) XPS survey spectrum of NiFe-LDH, (**d**) high-resolution spectra of Ni 2p, (**e**) Fe 2p, and (**f**) O1s for NiFe-LDH.
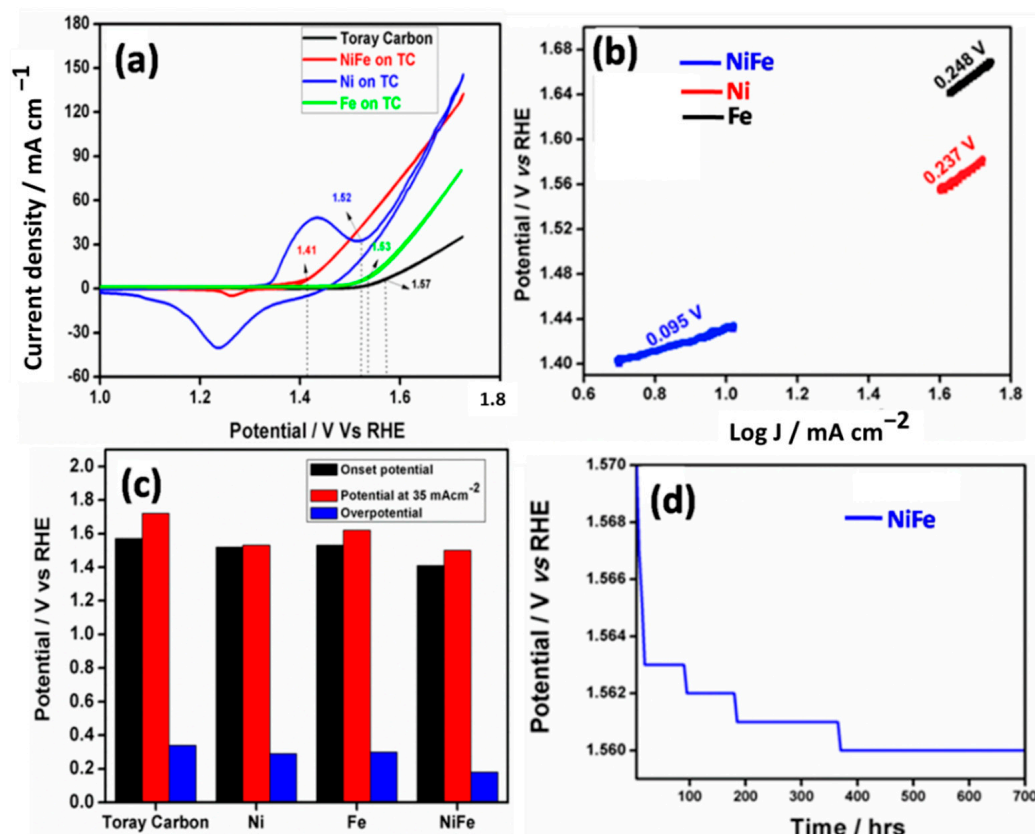
Figure 7. OER studies to evaluate performance of as-prepared samples. (**a**) LSV study of TC, Fe on TC, Ni on TC, and NiFe-LDH on TC tested in 1M KOH electrolyte solution with scan rate of 10 mV s^{-1}. (**b**) Tafel slope values of Fe on TC, Ni on TC, and NiFe-LDH on TC. (**c**) Comparison plot of the onset potential, the onset potential at 35 mA cm^{-2}, and the overpotential for TC, Fe on TC, Ni on TC, and NiFe-LDH on TC. (**d**) Stability test for NiFe-LDH on TC.

Figure 8 represents the electrochemical stability test and OER activity of Ni, Fe, and NiFe-LDH on TC at various temperatures (25, 55, and 85 °C). As-prepared NiFe-LDH on the TC electrocatalyst exhibited high stability for 700 h with the onset potential of 1.56 V at room temperature (25 °C). The onset potential suddenly dropped to 1.38 V at 85 °C and then is was maintain more stable. The reason for the dropped potential is that, if we consider the stability under high-temperature conditions, the temperature rise induces the molecular collision, thereby enhancing the kinetic energy to accelerate the activity, especially at higher overpotentials. However, this might not be the case in the lower overpotentials where the activation energy of the OER should be overcome even if it has more kinetic energy with high temperature. That is why more deviation was encountered at low overpotential regions. Additionally, with the temperature increment, it is common to have an increase in the kinetic energy that influences the activity when the potential is applied to the electrode/electrolyte interface. From this result, we observed that temperature is also one of the key factors to enhance the electrocatalytic activity of NiFe-LDH on TC for OER in an alkaline medium. Moreover, NiFe-LDH on TC nanomaterials becomes very stable and exhibited excellent OER performance at higher temperatures. This is the first time that the NiFe-LDH electrocatalyst showed high stability over 700 h at a higher temperature.
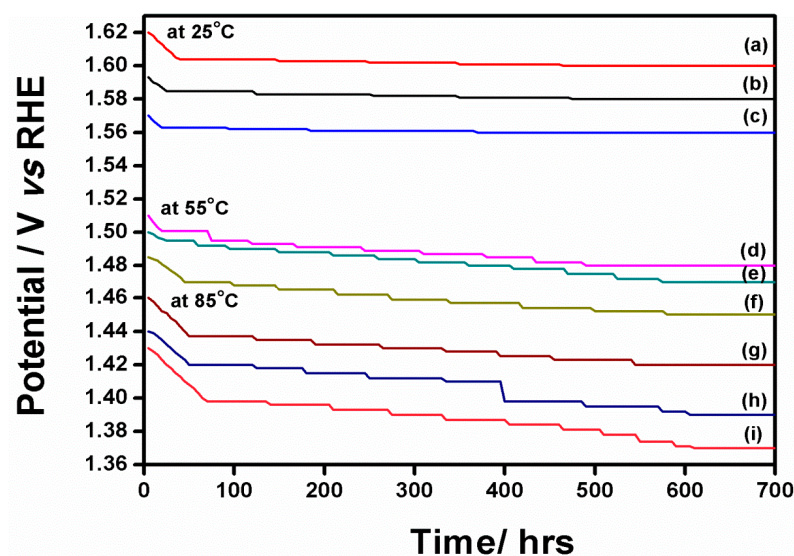
Figure 8. Chronopotentiometry measurement of (**a**) Ni on TC, (**b**) Fe on TC, and (**c**) NiFe-LDH on TC at 25 °C, (**d**) Ni on TC, (**e**) Fe on TC, and (**f**) NiFe-LDH on TC at 55 °C, and (**g**) Ni on TC, (**h**) Fe on TC, and (**i**) NiFe-LDH on TC at 85 °C.

3. Materials and Methods

3.1. Materials

All chemicals were purchased at ananalytic reagent grade for the experiment. Toray carbon (TC) sheets were received from Alfa Aesar, India. Nickel (II) sulfateheptahydrate ($NiSO_4 \cdot 7H_2O$), nickel (II) chloride hexahydrate ($NiCl_2 \cdot 6H_2O$), boric acid (H_3BO_3), potassium hydroxide, sodium lauryl sulphate, iron (II) sulfateheptahydrate ($FeSO_4 \cdot 7H_2O$), glycine, citric acid, and iron (II) chloride hexahydrate$FeCl_3 \cdot 6H_2O$ were supplied from Sigma Aldrich, India. Ultrapure water was used as a solvent for all the experimental processes.

3.2. Preparation of Fe Electrode

The electro deposition of iron (Fe) on TC was undertaken in a sulphate iron bath (350 g L^{-1} $FeSO_4 \cdot 7H_2O$, 10 g L^{-1} glycine, 2 g L^{-1} citric acid, and 0.05 g L^{-1} of sodium lauryl sulphate). The electrochemical deposition was carried out using Toray carbon as the cathode and an electrolytic-grade Fe sheet as the anode. The electrolyte bath was maintained at pH 2–2.5 (at room temperature) at a current density of 4 A dm^{-2} and 2 A dm^{-2} for 30min. The electrochemical deposition process leads to a thin brown film deposited on the TC.

3.3. Preparation of Ni Electrode

The electrochemical deposition of nickel (Ni) on Toray carbon was undertaken in a sulphate nickel bath (250 g L^{-1} $NiSO_4 \cdot 7H_2O$, 45 g L^{-1} $NiCl_2 \cdot 6H_2O$, 30 g L^{-1} H_3BO_3, and 0.05 g L^{-1} of sodium lauryl sulphate). The electrochemical deposition was carried out using TC as the cathode and an electrolytic-grade Ni sheet as the anode. The electrolyte bath was maintained at pH 4 (50 °C) at a current density of 6 A dm^{-2} and 8 A dm^{-2} for 30 min. The electrochemical deposition process leads to a thin silver film deposited on the TC.

3.4. Preparation of NiFe Electrode

The electrochemical deposition of NiFe on TC was undertaken in anickel iron sulphate bath (2–3 g L^{-1} $NiCl_2 \cdot 6H_2O$, 2.1 g L^{-1} $FeCl_3 \cdot 6H_2O$, and 25 g L^{-1} of H_3BO_3). The electrochemical deposition was carried out using TC as the cathode and an electrolytic-grade graphite sheet as the anode. The electrolyte bath was maintained at pH 2.5 (55 °C) at a current density of 2 A dm^{-2} for 30 min.

3.5. Characterization

The crystal structure and plane of Ni, Fe, and NiFe-LDH were carried out using the (D8 ADVANCE, Bruker, Bengaluru, Karnataka, India) X-ray diffractometer with Cu-Ká (ë = 1.5405 Å) radiation in the range of 20–80°. The Raman spectroscopy provided the information about the vibrational mode of molecules and the spectra were collected by Renishaw (Gloucestershire, UK) via Raman microscope with a 632.8 nm wavelength incident laser light. The structural morphology of as-prepared Ni, Fe, and NiFeLDH was investigated using FE-SEM (Carl Zeiss SUPRA 55V PFEI, Oberkochen, Germany) and HR-TEM (a FEI TECNAI G220 with an accelerating voltage of 200 kV, supplied from Sao Paulo, Brazil). The presence of elements was analyzed by the X-ray photoelectron spectroscopy (XPS) with a PHI 5000 Versa Probe ULVAC instrument (Chigasaki, Kanagawa, Japan).

4. Conclusions

In summary, we successfully used a facile route for the electrochemical deposition of the NiFe-LDH on TC as an electrocatalyst for the OER, which was an attractive method to control the morphology with (oxy)hydroxides phases. NiFe-LDH on the TC electrocatalyst showed the lowest onset potential (1.41 V) when compared to bare Ni (1.52 V) and Fe on TC (1.53 V) with the lowest Tafel value of 0.095 V dec^{-1} in the 1 M KOH electrolyte solution with ascan rate of 10 mV s^{-1}. Moreover, we tested the long-time stability of the NiFe-LDH on the TC electrocatalyst in the two-electrode system. The catalyst exhibited a high stability for 700 h with no change in the current density of 120 mA cm^{-2}. Hence, the NiFe-LDH on TC was demonstrated as a superior active and highly stable electrocatalyst in the OER from the water splitting at room temperature as well as high temperature. Therefore, it can be considered as a suitable electrocatalyst in the industrial-scale production of oxygen and hydrogen from water.

References

1. Seh, Z.W.; Kibsgaard, J.; Dickens, C.F.; Chorkendorff, I.; Norskov, J.K.; Jaramillo, T.F. Combining theory and experiment in electrocatalysis: Insights into materials design. *Science* **2017**, *355*, eaad4998. [CrossRef]
2. Peera, S.G.; Koutavarapu, R.; Liu, C.; Rajeshkhanna, G.; Asokan, A.; Reddy, C.V. Cobalt Nanoparticle-Embedded Nitrogen-Doped Carbon Catalyst Derived from a Solid-State Metal-Organic Framework Complex for OER and HER Electrocatalysis. *Energies* **2021**, *14*, 1320. [CrossRef]

3. Peera, S.G.; Koutavarapu, R.; Chao, L.; Singh, L.; Murugadoss, G.; Rajeshkhanna, G. 2D MXene Nanomaterials as Electrocatalysts for Hydrogen Evolution Reaction (HER): A Review. *Micromachines* **2022**, *13*, 1499. [CrossRef]
4. You, B.; Sun, Y. Innovative Strategies for Electrocatalytic Water Splitting. *Acc. Chem. Res.* **2018**, *51*, 1571. [CrossRef]
5. Song, F.; Bai, L.; Moysiadou, A.; Lee, S.; Hu, C.; Liardet, L.; Hu, X. Transition metal oxides as electrocatalysts for the oxygen evolution reaction in alkaline solutions: An application-inspired renaissance. *J. Am. Chem. Soc.* **2018**, *140*, 7748. [CrossRef]
6. Han, L.; Dong, S.; Wang, E. Transition-metal (Co, Ni, and Fe)-based electrocatalysts for the water oxidation reaction. *Adv. Mater.* **2016**, *28*, 9266. [CrossRef]
7. Benck, J.D.; Hellstern, T.R.; Kibsgaard, J.; Chakthranont, P.; Jaramillo, T.F. Catalyzing the hydrogen evolution reaction (HER) with molybdenum sulfide nanomaterials. *ACS Catal.* **2014**, *4*, 3957. [CrossRef]
8. Zhu, K.; Zhu, X.; Yang, W. Application of in situ techniques for the characterization of NiFe based oxygen evolution reaction (OER) electrocatalysts. *Angew. Chem. Int. Ed.* **2019**, *58*, 1252. [CrossRef]
9. Suen, N.T.; Hung, S.F.; Quan, Q.; Zhang, N.; Xu, Y.J.; Chen, H.M. Electrocatalysis for the oxygen evolution reaction: Recent development and future perspectives. *Chem. Soc. Rev.* **2017**, *46*, 337. [CrossRef]
10. Bediako, D.K.; Surendranath, Y.; Nocera, D.G. Mechanistic studies of the oxygen evolution reaction mediated by a nickel–borate thin film electrocatalyst. *J. Am. Chem. Soc.* **2013**, *135*, 3662. [CrossRef]
11. Jothi, V.R.; Bose, R.; Rajan, H.; Jung, C.; Yi, S.C. Harvesting electronic waste for the development of highly efficient eco-design electrodes for electrocatalytic water splitting. *Adv. Energy Mater.* **2018**, *8*, 1802615. [CrossRef]
12. Ng, J.W.D.; García-Melchor, M.; Bajdich, M.; Chakthranont, P.; Kirk, C.; Vojvodic, A.; Jaramillo, T.F. Gold-supported cerium-doped NiOx catalysts for water oxidation. *Nat. Energy* **2016**, *1*, 16053. [CrossRef]
13. Su, C.Y.; Cheng, H.; Li, W.; Liu, Z.Q.; Li, N.; Hou, Z.; Bai, F.Q.; Zhang, H.X.; Ma, T.Y. Atomic modulation of FeCo–nitrogen–carbon bifunctional oxygen electrodes for rechargeable and flexible all-solid-state zinc–air battery. *Adv. Energy Mater.* **2017**, *7*, 1602420. [CrossRef]
14. Chakrapani, K.; Ozcan, F.; Ortega, K.F.; Machowski, T.; Behrens, M. Composition-dependent effect of the calcination of cobalt, nickel and gallium based layered double hydroxides to mixed metal oxides in the oxygen evolution reaction. *ChemElectroChem* **2018**, *5*, 93. [CrossRef]
15. Yu, N.; Cao, W.; Huttula, M.; Kayser, Y.; Hoenicke, P.; Beckhoff, B.; Lai, F.; Dong, R.; Sun, H.; Geng, B. Fabrication of FeNi hydroxides double-shell nanotube arrays with enhanced performance for oxygen evolution reaction. *Appl. Catal. B Environ.* **2020**, *261*, 118193. [CrossRef]
16. Corrigan, D.A.; Conell, R.S.; Fierro, C.A.; Scherson, D.A. In Situ Mossbauer study of redox processes in a composite hydroxide of iron and nickel. *J. Phys. Chem.* **1987**, *91*, 5009. [CrossRef]
17. Su, X.; Wang, Y.; Zhou, J.; Gu, S.; Li, J.; Zhang, S. Operando spectroscopic identification of active sites in NiFeprussian blue analogues as electrocatalysts: Activation of oxygen atoms for oxygen evolution reaction. *J. Am. Chem. Soc.* **2018**, *140*, 11286. [CrossRef]
18. Song, F.; Busch, M.M.; Lassalle-Kaiser, B.; Hsu, C.S.; Petkucheva, E.; Bensimon, M.; Chen, H.M.; Corminboeuf, C.; Hu, X. An unconventional iron nickel catalyst for the oxygen evolution reaction. *ACS Central. Sci.* **2019**, *5*, 558. [CrossRef]
19. Chung, D.Y.; Lopes, P.P.; Martins, P.F.B.D.; He, H.; Kawaguchi, T.; Zapol, P.; You, H.; Tripkovic, D.; Strmcnik, D.; Zhu, Y.; et al. Dynamic stability of active sites in hydr(oxy) oxides for the oxygen evolution reaction. *Nat. Energy* **2020**, *5*, 222. [CrossRef]
20. Hu, Q.; Li, G.M.; Liu, X.F.; Zhu, B.; Chai, X.Y.; Zhang, Q.L.; Liu, J.H.; He, C.X. Superhydrophilic phytic acid-doped conductive hydrogels as metal-free and binder-free electrocatalysts for efficient water oxidation. *Angew. Chem. Int. Edit.* **2019**, *58*, 4318. [CrossRef]
21. Han, X.P.; Zhang, W.; Ma, X.Y.; Zhong, C.; Zhao, N.Q.; Hu, W.B.; Deng, Y.D. Identifying the activation of bimetallic sites in NiCo$_2$S$_4$@gC$_3$N$_4$-CNT hybrid electrocatalysts for synergistic oxygen reduction and evolution. *Adv. Mat.* **2019**, *31*, 1808281. [CrossRef]
22. Wang, W.; Lu, Y.; Zhao, M.; Luo, R.; Yang, Y.; Peng, T.; Yan, H.; Liu, X.; Luo, Y. Controllable tuning of cobalt nickel-layered double hydroxide arrays as multifunctional electrode for flexible supercapattery device and oxygen evolution reaction. *ACS Nano* **2019**, *13*, 12206. [CrossRef]
23. Xiang, Q.; Li, F.; Chen, W.; Ma, Y.; Wu, Y.; Gu, X.; Qin, Y.; Tao, P.; Song, C.; Shang, W.; et al. In-situ vertical growth of Fe-Ni layered double hydroxide arrays on Fe-Ni alloy foil: Interfacial layer enhanced electrocatalyst with small overpotential for oxygen evolution reaction. *ACS Energy Lett.* **2018**, *3*, 2357. [CrossRef]
24. Rashid, J.; Parveen, N.; Haq, T.; Iqbal, A.; Talib, S.H.; Awan, S.U.; Hussain, N.; Zaheer, M. g-C$_3$N$_4$/CeO$_2$/Fe$_3$O$_4$ ternary composite as an efficient bifunctional catalyst for overall water splitting. *ChemCatChem* **2018**, *10*, 5587. [CrossRef]
25. Xu, H.; Cao, J.; Shan, C.; Wang, B.; Xi, P.; Liu, W.; Tang, Y. MOF-merived hollow CoS decorated with CeO$_x$ nanoparticles for boosting oxygen evolution reaction electrocatalysis. *Angew. Chem.* **2018**, *130*, 8790. [CrossRef]
26. Demir, E.; Akbayrak, S.; Onal, A.M.; Ozkar, S. Nanoceria-supported ruthenium(0) nanoparticles: Highly active and stable catalysts for hydrogen evolution from water. *ACS Appl. Mater. Interfaces* **2019**, *534*, 704. [CrossRef]
27. Yu, J.; Cao, Q.; Li, Y.; Long, X.; Yang, S.; Clark, J.K.; Nakabayashi, M.; Shibata, N.; Delaunay, J.J. Defect-rich NiCeO$_x$ electrocatalyst with ultrahigh stability and low overpotential for water oxidation. *ACS Catal.* **2019**, *9*, 1605. [CrossRef]

28. Kaleeswarran, P.; Praveen Kumar, M.; Mangalaraja, R.V.; Hartley, U.W.; Sasikumar, M.; Venugopalan, R.; Rajesh Kumar, M.; Rajabathar, J.R.; Peera, S.G.; Murugadoss, G. FeTiO$_3$ Perovskite Nanoparticles for Efficient Electrochemical Water Splitting. *Catalysts* **2021**, *11*, 1028. [CrossRef]

29. Zaman, S.; Tian, X.; Su, Y.Q.; Cai, W.; Yan, Y.; Qi, R.; Douka, A.I.; Chen, S.; You, B.; Liu, H.; et al. Direct integration of ultralow-platinum alloy into nanocarbon architectures for efficient oxygen reduction in fuel cells. *Sci. Bull.* **2021**, *66*, 2207. [CrossRef]

30. Ali, H.; Zaman, S.; Majeed, I.; Kanodarwala, F.K.; Amtiaz Nadeem, M.; Stride, J.A.; Nadeem, M.A. Porous carbon/rGO composite: An ideal support material of highly efficient palladium electrocatalysts for the formic acid oxidation reaction. *ChemElectroChem* **2017**, *4*, 3126. [CrossRef]

31. Li, M.F.; Huang, L.; Zaman, S.; Guo, W.; Liu, H.; Guo, X.; Xia, B.Y. Corrosion chemistry of electrocatalysts. *Adv Mater.* **2022**. [CrossRef]

32. Zaman, S.; Wang, M.; Liu, H.; Sun, F.; Yu, Y.; Shui, J.; Chen, M.; Wang, H. Carbon-based catalyst supports for oxygen reduction in proton-exchange membrane fuel cells. *Trends Chem.* **2022**, *4*, 886. [CrossRef]

33. Zaman, S.; Su, Y.Q.; Dong, C.L.; Qi, R.; Huang, L.; Qin, Y.; Huang, Y.C.; Li, F.M.; You, B.; Guo, W.; et al. Scalable molten salt synthesis of platinum alloys planted in metal–nitrogen–graphene for efficient oxygen reduction. *Angew. Chem. Int. Ed.* **2022**, *61*, 202115835. [CrossRef]

34. Lu, X.; Zhao, C. Electro deposition of hierarchically structured three-dimensional nickel–iron electrodes for efficient oxygen evolution at high current densities. *Nat. Commun.* **2015**, *6*, 6616. [CrossRef]

35. Novala, V.E.; Carriazoa, J.G. Fe$_3$O$_4$-TiO$_2$ and Fe$_3$O$_4$-SiO$_2$ core-shell powders synthesized from industrially processed magnetite (Fe$_3$O$_4$) microparticles. *Mater. Res.* **2019**, *22*, e20180660. [CrossRef]

36. Fei, J.; Zhao, J.; Du, C.; Ma, H.; Zhang, H.; Li, J. The facile 3D self-assembly of porous iron hydroxide and oxide hierarchical nanostructures for removing dyes from wastewater. *J. Mater. Chem. A* **2013**, *1*, 10300. [CrossRef]

37. Pramana, Y.B.; Setiawan, B.; Prihono, P.; Utomo, Y.; Subandowo, M.; Budipramana, K. A simple synthesis of nickel oxide nanotube using high voltage electrolysis. *J. Neutrino: J. Fis. Apl.* **2020**, *13*, 13. [CrossRef]

38. Gao, Y.; Zhao, Z.; Jia, H.; Yang, X.; Lei, X.; Kong, X.; Zhang, F. Partially reduced Ni^{2+}, Fe^{3+}-layered double hydroxide for ethanol electrocatalysis. *J. Mater Sci.* **2019**, *54*, 14515. [CrossRef]

39. Yang, Q.; Li, T.; Lu, Z.; Sun, X.; Liu, J. Hierarchical construction of an ultrathin layered double hydroxide nanoarray for highly-efficient oxygen evolution reaction. *Nanoscale* **2014**, *6*, 11789. [CrossRef]

40. Ali-Löytty, H.; Louie, M.W.; Singh, M.R.; Li, L.; Sanchez Casalongue, H.G.; Ogasawara, H.; Crumlin, E.J.; Liu, Z.; Bell, A.T.; Nilsson, A.; et al. Ambient-pressure XPS study of a Ni−Fe electrocatalyst for the oxygen evolution reaction. *J. Phys. Chem. C* **2016**, *120*, 2247. [CrossRef]

41. Praveen Kumar, M.; Murugesan, P.; Vivek, S.; Ravichandran, S. NiWO$_3$ Nanoparticles Grown on Graphitic Carbon Nitride (g-C$_3$N$_4$) Supported Toray Carbon as an Efficient Bifunctional Electrocatalyst for Oxygen and Hydrogen Evolution Reactions. *Part. Part. Syst. Charact.* **2017**, *34*, 1700043. [CrossRef]

42. Gao, R.; Yan, D. Fast formation of single-unit-cell-thick and defect-rich layered double hydroxide nanosheets with highly enhanced oxygen evolution reaction for water splitting. *Nano Res.* **2018**, *11*, 1883. [CrossRef]

43. He, Z.; Zhang, J.; Gong, Z.; Lei, H.; Zhou, D.; Zhang, N.; Mai, W.; Zhao, S.; Chen, Y. Activating lattice oxygen in NiFe-based (oxy)hydroxide for water electrolysis. *Nat Commun.* **2022**, *13*, 2191. [CrossRef] [PubMed]

44. Pascuzzi, M.E.C.; Man, A.J.W.; Goryachev, A.; Hofmann, J.P.; Hensen, E.J.M. Investigation of the stability of NiFe-(oxy)hydroxide anodes in alkaline water electrolysis under industrially relevant conditions. *Catal. Sci. Technol.* **2020**, *10*, 5593–5601. [CrossRef]

45. Li, X.; Liu, C.; Fang, Z.; Xu, L.; Lu, C.; Hou, W. Ultrafast room-temperature synthesis of self-supported NiFe-layered double hydroxide as large-current–density oxygen evolution electrocatalyst. *Small* **2022**, *18*, 2104354. [CrossRef]

46. Louie, M.W.; Bell, A.T. An Investigation of thin-film Ni−Fe oxide catalysts for the electrochemical evolution of oxygen. *J. Am. Chem. Soc.* **2013**, *135*, 12329–12337. [CrossRef]

47. Dong, J.; Wang, Y.; Jiang, Q.; Nan, Z.-A.; Fan, F.R.; Tian, Z.-Q. Charged droplet-driven fast formation of nickel–Iron (oxy)hydroxides with rich oxygen defects for boosting overall water splitting. *J. Mater. Chem. A* **2021**, *9*, 20058–20067. [CrossRef]